ANNUAL REVIEWS

Annual Review of Pharmacology and Toxicology

Cryo-Electron Microscopy: Moving Beyond X-Ray Crystal Structures for Drug Receptors and Drug Development

Javier García-Nafría[1,2] and Christopher G. Tate[1]

[1]MRC Laboratory of Molecular Biology, Cambridge CB2 0QH, United Kingdom; email: cgt@mrc-lmb.cam.ac.uk

[2]Current affiliation: Institute for Biocomputation and Physics of Complex Systems (BIFI) and Laboratorio de Microscopias Avanzadas, University of Zaragoza, 50018 Zaragoza, Spain; email: jgarcianafria@unizar.es

Annu. Rev. Pharmacol. Toxicol. 2020. 60:51–71

First published as a Review in Advance on July 26, 2019

The *Annual Review of Pharmacology and Toxicology* is online at pharmtox.annualreviews.org

https://doi.org/10.1146/annurev-pharmtox-010919-023545

Keywords

cryo-EM, GPCR, $GABA_A$ receptor, X-ray crystallography, drug development

Abstract

Electron cryo-microscopy (cryo-EM) has revolutionized structure determination of membrane proteins and holds great potential for structure-based drug discovery. Here we discuss the potential of cryo-EM in the rational design of therapeutics for membrane proteins compared to X-ray crystallography. We also detail recent progress in the field of drug receptors, focusing on cryo-EM of two protein families with established therapeutic value, the γ-aminobutyric acid A receptors ($GABA_ARs$) and G protein–coupled receptors (GPCRs). $GABA_ARs$ are pentameric ion channels, and cryo-EM structures of physiological heteromeric receptors in a lipid environment have uncovered the molecular basis of receptor modulation by drugs such as diazepam. The structures of ten GPCR–G protein complexes from three different classes of GPCRs have now been determined by cryo-EM. These structures give detailed insights into molecular interactions with drugs, GPCR–G protein selectivity, how accessory membrane proteins alter receptor–ligand pharmacology, and the mechanism by which HIV uses GPCRs to enter host cells.

INTRODUCTION

Membrane proteins account for 20–30% of the human genome (1, 2) and have great therapeutic value since they are the target for approximately 60% of the drugs used in the clinic (3). Structural information is a key component in the rational design of drugs, providing a platform to increase the success rate of computational modelling used to design and improve drug specificity and potency (4). Until recently, the only method to obtain protein structures of receptors was X-ray crystallography, which, for membrane proteins, requires heroic efforts and has limited success rates. Cryo-electron microscopy (cryo-EM) offers several advantages over X-ray crystallography and has revolutionized structural biology of membrane proteins, providing fundamental insights into both the molecular mechanisms of membrane receptors and the binding modes of therapeutic drugs. Examples of this progress include the structures of γ-secretase (5, 6), the cystic fibrosis transmembrane conductance regulator (7, 8), the hERG K^+ channel (9), and a chimera of the voltage-gated sodium channel $Na_v1.7$ (10). There are many other recent reviews on aspects of cryo-EM, including progress in the structural biology of ion channels (11, 12) and G protein–coupled receptors (GPCRs) (13–17), technical improvements in cryo-EM (18–21), and aspects of drug discovery (22–26). Here we discuss cryo-EM methodology, with a focus on its use for structure-based drug discovery (SBDD) of membrane proteins, and the recent burst of structural information on two classes of drug receptors of established therapeutic value, namely the γ-aminobutyric acid A receptors ($GABA_A$Rs) and GPCRs.

CRYO-ELECTRON MICROSCOPY AND DRUG DISCOVERY

Cryo-Electron Microscopy as a Structural Biology Technique

Cryo-EM has become the method of choice to obtain structural information on drug receptors and has several advantages when compared to macromolecular crystallography. X-ray crystallography demands milligram amounts of a pure and homogenous sample, which must be stable enough to withstand days in a crystallization solution. Crucially, the protein must then form crystals with well-ordered arrays of molecules held together by protein–protein contacts; the quality of the crystals dictates the quality of the diffraction pattern and hence the resolution of the determined structure. Unfortunately, membrane proteins are notoriously difficult to grow into well-ordered crystals, due to their instability in detergents suitable for crystallization, their flexibility, and their lack of hydrophilic areas to make strong contacts between molecules in the crystal lattice. In addition, membrane proteins can be difficult to overexpress and purify in a native conformation. Consequently, the structure determination of membrane proteins has lagged behind that of soluble proteins. However, with the advent of the so-called cryo-EM resolution revolution (27), structures can now be obtained by cryo-EM using microgram amounts of a protein sample, which is directly vitrified on cryo-grids after purification and without the need to form crystals. In addition, very mild detergents that are unsuitable for X-ray crystallography can be used for the purification of even quite unstable membrane proteins (28), allowing structures of previously intractable targets to be determined. However, it must be stressed that the quality of the sample is still the most critical factor in high-resolution structural determination by cryo-EM, which requires crystallization-quality material at the time of vitrification. In fact, the number of cryo-EM images required and the resolution attained appear to correlate with sample quality and follow the same rules as in crystallography, where the stabilization of constructs and removal of flexible loops can significantly influence the final resolution (29).

In a typical single-particle cryo-EM experiment, the protein sample is vitrified on cryo-grids, which are then imaged using a 200–300 kV transmission electron microscope. Images are collected using direct electron detectors, which have increased sensitivity and speed compared to film, allowing the collection of tens of frames per image, each with a limited amount of electron dose (30). The ability to split the image into frames allows computer software to preserve the high-resolution information of the images by correcting for stage drift and beam-induced motion during image processing (31, 32). It also allows for the correction of radiation damage by down-weighting information in a resolution-dependent manner in each frame (31, 33). The inclusion of maximum likelihood approaches to cryo-EM data processing (34) (and other processing tools) enabled the separation of conformationally heterogeneous samples, purifying in silico distinct homogenous conformations that can be refined to high resolution. Further developments in software have focused on eliminating fine errors in data collection that have a significant impact when moving toward atomic resolution. These developments include estimations of defocus for each particle in a micrograph (35–37), performing Ewald sphere correction (35, 38), and beam tilt correction (35, 39). The interested reader is referred to several excellent in-depth reviews on advancements in electron microscopy (18, 21, 40, 41).

Despite the wonderful success of cryo-EM, there are still limitations and bottlenecks associated with structure determination. Although crystals are not required, cryo-grids must be well populated with intact protein particles in random orientations. In the time between sample application onto the grid and vitrification (typically about 1 s), a protein molecule will hit the air–water interface between 100 and 1,000 times (42, 43), potentially promoting preferential orientation or protein aggregation. For some samples, this will prevent structure determination. A number of solutions can reduce the problem of preferred orientations of the sample on the grid, including reducing the time from blotting to freezing (44), adding certain additives (8) or antibodies (45, 46), using different supports on the cryo-grid [e.g., carbon, graphene, or graphene oxide (47)], or making a slight change in the protein construct. Cryo-EM projects can be stalled for months or even years due to the preferred orientations problem, and new solutions are required to make cryo-EM usable for any protein sample.

A technology that is increasingly being used for cryo-EM data collection is the Volta phase plate (VPP) (48). The VPP is a film of amorphous carbon (typically about 10 nm thick) placed after the sample in the electron microscope, which enhances image contrast through inducing a phase shift in the electron beam, thus boosting the signal-to-noise ratio of the protein particles (**Figure 1*a***). The VPP has been used to determine structures of proteins as small as 64 kDa (49) and has been shown to produce similar resolutions with less data (50–52). This was seen recently in the determination of the structure of human A_{2A} receptor in complex with the G_s heterotrimer (53), where images containing 145,000 particles collected using a VPP were sufficient to attain a resolution of 4.88 Å. A B-factor plot, which describes the increase in resolution as a function of the amount of data (**Figure 1*b***), suggested that approximately 5 million particles collected without a VPP would be required to attain a similar resolution, requiring about 65 days of data collection on the particular Titan Krios microscope. The VPP has been used to determine the structure of many membrane proteins, including GPCR–G protein complexes and $GABA_A$Rs (see below) (45, 46, 54–58). However, the increased difficulty in data collection and the variability in behavior between different VPPs make this technology far from routine. The fact that high-resolution structures can also be obtained for small proteins without using a VPP (59) generates uncertainty in the cryo-EM community regarding the best data collection strategy. Further studies are required to establish the true potential of a VPP and the circumstances under which a VPP has the most impact on improving the determination of protein structures.

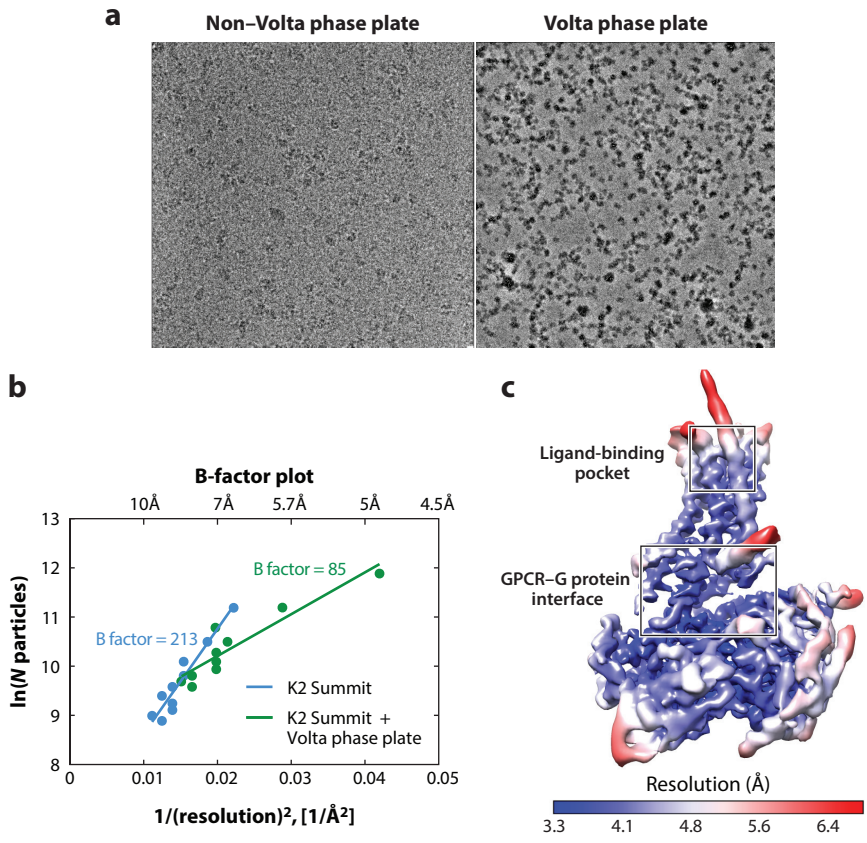

Figure 1

Cryo-electron microscopy (cryo-EM) methodology with and without a Volta phase plate (VPP). (*a*) A side-by-side comparison of (*left*) a standard defocus micrograph and (*right*) a micrograph taken with a VPP. (*b*) A B-factor plot showing the difference between cryo-EM data collected with and without a VPP for the A_{2A} receptor ($A_{2A}R$) in complex with a G_s heterotrimer. (*c*) Example of local resolution, showing the cryo-EM map of the $A_{2A}R$–G_s heterotrimer. Figure adapted with permission from Reference 53.

Cryo-Electron Microscopy in the Use of Structure-Based Drug Discovery: State-of-the-Art Techniques and Limitations

SBDD relying on X-ray crystallography requires the production of reproducible diffracting crystals with different compounds. However, for the case of membrane proteins, obtaining reproducible-quality crystals can be challenging, and, in many cases, a single crystal out of hundreds is found to be suitable for structure determination. A solution to this has been the thermostabilization of receptors, often applied to G protein–coupled receptors (60, 61), an approach that has been successful in yielding receptor constructs amenable to high-throughput X-ray crystallography (62). However, this approach still requires the stabilization of receptors by mutagenesis, the production of large amounts of protein sample, and crystallization.

Cryo-EM now provides an attractive alternative to X-ray crystallography for the visualization of drug-binding modes. Proof-of-principle has been done mostly for soluble protein systems, with examples that include the isocitrate dehydrogenase complexed with a compound with potential in cancer treatment (ML309) (63) and the structure of the *Plasmodium falciparum* 20S proteasome in

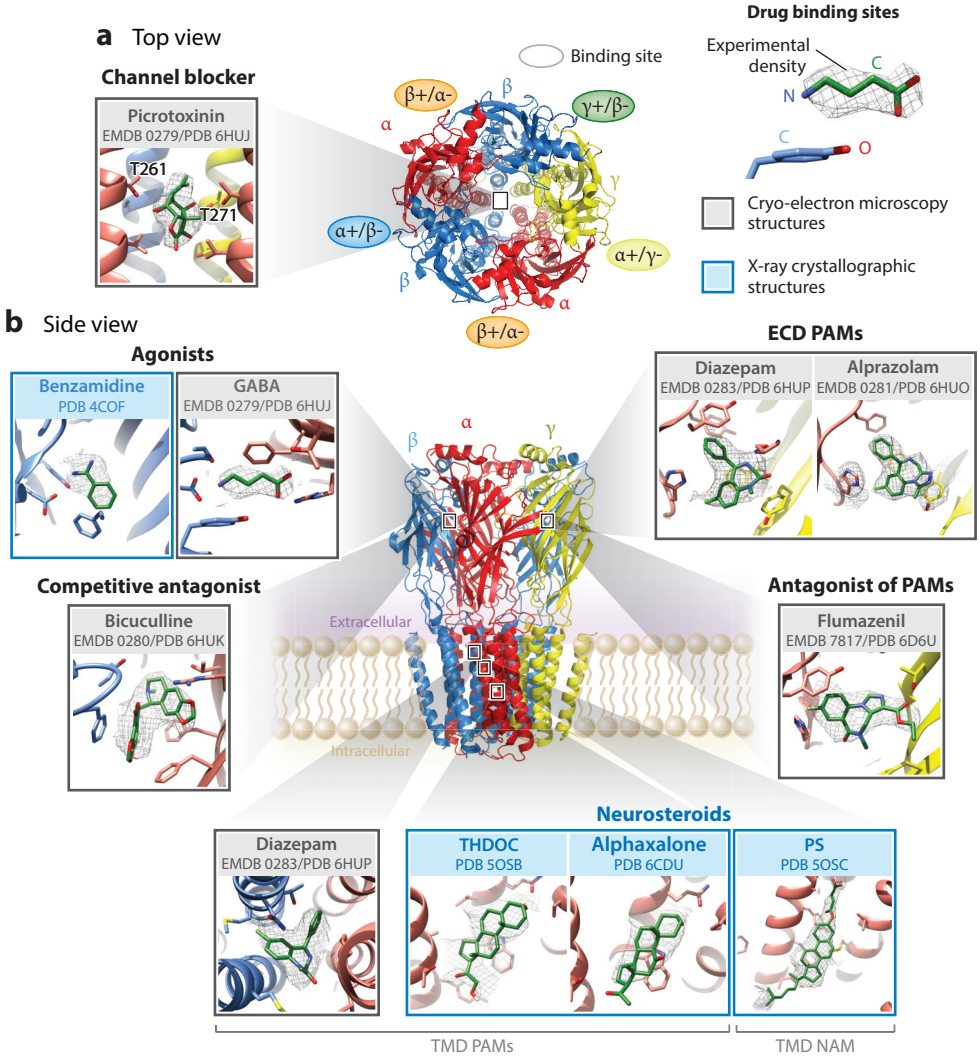

Figure 2

Structure of the prototypical $GABA_AR$ with insights into drug-binding modes, viewed from (*a*) the extracellular surface and (*b*) within the membrane plane. In both panels, the prototypical $GABA_AR$ is composed of α (*red*), β (*blue*), and γ (*yellow*) subunits. Binding sites for drugs are depicted, and the insets show experimental density and the drugs represented as sticks (C, *green*; O, *red*; N, *dark blue*). Carbon atoms from receptor residues are colored according to the subunit coloring scheme described above. Experimental density is clipped to the ligand (*gray mesh*), and X-ray crystallographic structures (*light blue*) and cryo-electron microscopy structures (*gray*) are shown. Abbreviations: ECD, extracellular domain; GABA, γ-aminobutyric acid; $GABA_AR$, $GABA_A$ receptor; PS, pregnenolone sulfate; PAM, positive allosteric modulator; NAM, negative allosteric modulator; THDOC, tetrahydrodeoxycorticosterone; TMD, transmembrane domain.

complex with WLW vinyl sulfone, an inhibitor of the malarial proteasome that does not bind to the human proteasome (64, 65). In the case of membrane proteins, the greatest progress was initially made with the TRPV1 channel, which was the first membrane protein to achieve high-resolution information by cryo-EM (66); its structure was later solved while embedded in a lipid nanodisc, showing the binding of capsazepine and resiniferatoxin (67). Cryo-EM is now providing great

insights into membrane proteins and compounds of high therapeutic value (see below); however, it still has some limitations that need to be fixed in order for it to be used routinely in SBDD.

Limitations for the Use of Cryo-Electron Microscopy in Structure-Based Drug Discovery

SBDD is being applied to develop novel therapeutics to membrane protein targets using X-ray crystallography (68, 69), which entails the determination of the structure of the target protein bound to compounds under development as drugs. Medicinal chemists can then use the structures to suggest modifications that improve affinity and specificity. This is an iterative cycle that can require hundreds of structures to be determined. Crystal growth, crystal harvesting, data collection, and structure solution can all be streamlined, although this may take years of work for a GPCR. A significant advantage of X-ray crystallography is that molecular replacement can be used to rapidly determine structures of a target bound to different ligands. In the most favorable cases, this can be achieved with a GPCR (70), although the throughput is considerably lower than what is possible for some soluble proteins (71).

Several bottlenecks currently prevent cryo-EM from generating similar amounts of data in a short time. First, data collection is orders of magnitude slower in cryo-EM than in crystallography, frequently requiring several days of data collection to reach a useful resolution for SBDD. Second, although a few cryo-EM structures have been determined to better than 2-Å resolution, membrane protein structures are normally determined in the range of 3–4-Å resolution. This could improve significantly with the development of faster and better hardware and software. Third, data processing demands extensive computational time, even with the implementation of parallel processing using graphics processing units (72). Lastly, there is a lack of automation in data processing because significant user skill is currently required to obtain the best resolution from a given set of cryo-EM data (73) using the most-used software packages (35, 74), although automated systems are under development (75). Since resolution is normally limiting and map density for small molecules tends to be noisy, it is imperative to obtain the best map possible if SBDD from cryo-EM data is to become a reality.

Another aspect of cryo-EM structure determination that requires human expertise is map interpretation. The currently used Fourier Shell Correlation resolution estimation does not necessarily correspond exactly with the quality of the map density, and the term modelability has been introduced to judge the quality of a model based on how easily atomic coordinates can be generated from the map (76). Cases where maps containing fewer particles (and slightly less resolution) produce an improved quality of map are not uncommon, although the reason behind this phenomenon is unclear. Therefore, it is up to the scientist to perform an assessment to obtain the best final map possible.

Once the final cryo-EM map is available, it should not be judged by the overall resolution. The local resolution can vary greatly within different regions of the map, and when assessing how drugs bind to a receptor, the resolution of the drug-binding pocket should be taken into account rather than the global resolution. As an example, cryo-EM structures of GPCRs normally have higher resolution at the GPCR–G protein interface and lower resolution at the distal extracellular site where the ligand-binding site is located (**Figure 1*c***).

CASE STUDY 1: $GABA_A$ RECEPTORS

Introduction to $GABA_A$ Receptors and Their Pharmacology

$GABA_A$Rs mediate inhibitory neurotransmission in the mammalian central nervous system (77–79), and receptor dysfunction results in a variety of neurological and psychiatric disorders,

including epilepsy, insomnia, anxiety, and autism (80). $GABA_A$Rs have a rich pharmacology: They are the targets for two types of endogenous molecules [GABA and neurosteroids (81, 82)] and a number of exogenous drugs with therapeutic, recreational, and illicit use (83, 84) such as anesthetics (85), benzodiazepines (86), barbiturates (87), and ethanol (88). Several factors contribute to the extensive pharmacology of $GABA_A$Rs. First, physiological $GABA_A$Rs are heteropentameric receptors composed from five out of potentially 19 different subunits in humans: six α subunits; three β subunits; three γ subunits; three ρ subunits; and one each of the ε, δ, θ, and π subunits (78, 89). The combination and arrangement of the different subunits determine receptor functionality and pharmacology. Most synaptic $GABA_A$Rs are formed by 2α, 2β, and 1γ subunits (78) arranged γ-β-α-β-α counterclockwise around the central pore axis when viewed from the extracellular surface (**Figure 2*a***). Many regulatory molecules have specificity for certain types of isoforms (90). For example, benzodiazepines require the γ subunit to be present; neurosteroids require α subunits (82); and classical benzodiazepines such as diazepam (Valium) and alprazolam (Xanax) bind specifically to α1, α2, α3, or α5 subunits but not to α4 or α6 subunits (91, 92). Secondly, each receptor subunit is composed of an extracellular hydrophilic domain (ECD), where the neurotransmitter binds, and a transmembrane domain (TMD), which forms the channel (93). Both the ECD and the TMD contain several binding sites for endogenous and exogenous regulatory molecules. The orthosteric and allosteric sites are normally found at the interface between subunits and are formed by the contribution of a principal face (+) from one subunit and a complementary face (−) from the adjacent subunit. Therefore, for a prototypical $GABA_A$R (formed by 2α, 2β, and 1γ subunits), there are four different binding sites at the ECD and four potential sites at the TMD (**Figure 2**). Knowledge about the binding mode and modulatory mechanism in which agonists and diverse regulatory molecules bind and modulate the function of $GABA_A$Rs has enormous physiological and therapeutic value and has been sought for many years.

From Crystals to Cryo-Electron Microscopy Structures in $GABA_A$ Receptors

Initial work on the structure determination of $GABA_A$Rs relied on the crystallization of homomeric receptors as model systems. The crystal structure of the homomeric β3 receptor was the first experimental model, providing a framework to study $GABA_A$R function and explain disease-causing mutations (94). Later efforts focused on obtaining insights into neurosteroid-binding modes to the TMD, since this could still be done using homomeric systems. Structural determination of such complexes by X-ray crystallography required extensive protein engineering of the receptor, with the α1 TMD of $GABA_A$Rs that contains the neurosteroid binding site fused to the ECD of the *Gloeobacter* ligand-gated ion channel (GLIC) (95), *Erwinia* ligand-gated ion channel (ELIC) (96), or $GABA_A$R β3 subunit (97). This resulted in structures that suggested how the anesthetic alphaxalone binds (96) and how positive and negative modulatory neurosteroids bind (95, 97). While positive allosteric modulators bound between subunits near the lipid interface [alphaxalone, tetrahydrodeoxycorticosterone (THDOC), and pregnanolone], the negative allosteric modulators bound at a discrete intrasubunit site (pregnenolone sulfate) (**Figure 2*b***).

Although the crystal structures of $GABA_A$ homomeric channels added significantly to our understanding of $GABA_A$Rs, they were far from ideal models. Heteromeric channels are the predominant form in vivo, and their complex pharmacology could only be unraveled from heteromeric structures. Cryo-EM has now made it possible to determine the structures of heteromeric $GABA_A$Rs, which would not have been possible using X-ray crystallography. A summary of these structures is found in **Table 1** and includes heteromers of α5β3 (98), α1β1γ2S (99), α1β2γ2 (100), and α1β3γ2L (45, 46) in complex with compounds such as GABA, flumazenil, picrotoxin, bicuculline, and benzodiazepines (**Figure 2**). Binding of GABA at the two β+/α− sites

Table 1 $GABA_A$ receptor and GPCR structures determined by cryo-electron microscopy

Protein	Detergent or nanodisc	Ligand	Type of ligand	PDB/EMDB	Overall Res^n (Å)	Number of images	Number of particles	Reference
$GABA_AR$ construct								
β3 homomer*	DMNG + CHS	Benzamidine	Agonist	4COF	3	NA	NA	94
β3/α5 chimera*	DDTM	No ligand	NA	5OJM	3.3	NA	NA	97
β3/α5 chimera*	DDTM	Pregnanolone	PAM	5O8F	3.2	NA	NA	97
GLIC-$GABA_AR$ α1 chimera*	DDM, CHS	No ligand	NA	5OSA	2.8	NA	NA	95
GLIC-$GABA_AR$ α1 chimera*	DDM, CHS	THDOC	PAM	5OSB	3.8	NA	NA	95
GLIC-$GABA_AR$ α1 chimera*	DDM, CHS	PS	NAM	5OSC	3.0	NA	NA	95
ELIC-α1$GABA_AR$ chimera*	DDM	Alphaxalone	PAM	6CDU	3.4	NA	NA	96
ELIC-α1$GABA_AR$ chimera*	DDM	Apo	NA	6D1S	3.2	NA	NA	96
α1β2γ2	DDM, CHS	GABA + flumazenil	Agonist + PAM antagonist	6D6T/7816	3.9	5,594	200,442	100
α1β2γ2	DDM, CHS	GABA + flumazenil	Agonist + PAM antagonist	6D6U/7817	3.9	5,594	292,662	100
α1β1γ2S	DDM + CHS	GABA	Agonist	6DW0/8922	3.8	1,391	49,417	99
α1β1γ2S	DDM + CHS	GABA	Agonist	6DW1/8923	3.1	1,391	68,229	99
α5β3	LMNG + CHS	GABA	Agonist	6A96/6998	3.5	3,724	161,455	98
α1β3γ2L	Nanodisc	GABA + PTX	Agonist + channel blocker	6HUJ/0279	3.0	794	67,604	45
α1β3γ2L	Nanodisc	PTX	Channel blocker	6HUG/0275	3.1	803	56,269	45
α1β3γ2L	Nanodisc	BCC	Competitive antagonist	6HUK/0280	3.7	988	30,536	45
α1β3γ2L	Nanodisc	ALP + GABA	PAM + agonist	6HUO/0282	3.3	815	39,050	45
α1β3γ2L	Nanodisc	DZP + GABA	PAM + agonist	6HUP/0283	3.6	768	55,077	45
α1β3γ2L	Nanodisc	No ligand	NA	6I53/4411	3.2	784	55,559	46
GPCRs								
CTR–G_s	LMNG + CHS	Calcitonin	Agonist	6NIY/9382	3.3	2,780	417,949	118
GLP-1–G_s	LMNG + CHS + GDN + POPG	GLP-1	Agonist	5VAI/653	4.1	17,332	139,299	119
GLP-1–G_s	LMNG + CHS	Exendin-P5	Agonist	6B3J/7039	3.3	2,793	184,672	56
$A_{2A}R$–G_s	LMNG	NECA	Agonist	6GDG/4390	4.1	827	128,002	53
5-HT_{1B}–G_o	DM	Donitriptan	Agonist	6G79/4358	3.8	5,737	730,118	54
MOR–G_i	LMNG + GDN + CHS	DAMGO	Agonist	6DDE/7868	3.5	2,642	359,406	121

(*Continued*)

Table 1 (*Continued*)

Protein	Detergent or nanodisc	Ligand	Type of ligand	PDB/EMDB	Overall Res^n (Å)	Number of images	Number of particles	Reference
Opsin–G_i	Digitonin	ATR	Agonist	6CMO/7517	4.5	19,368	227,386	120
A_1R–G_i	LMNG + CHS	Adenosine	Agonist	6D9H/7835	3.6	3,220	263,321	55
CB_1–G_i	LMNG + GDN + CHS	FUB	Agonist	6N4B/0339	3.5	2,759	177,787	122
CGRPR–G_s	LMNG + CHS	CGRP	Agonist	6E3Y/8978	3.3	3,180	407,000	58
CCR5-gp120–CD41	DDM + LMNG + CHS	No ligand	NA	6MEO/9108	3.9	10,530	307,346	128
mGluR5	GDN	L-quisqualate	Agonist	6N51/0345	4.0	5,391	123,096	124
mGluR5	Nanodisc	No ligand	NA	6N52/0346	4.0	1,984	73,472	124

Asterisks correspond to X-ray crystal structures included for comparative purposes, and proteins without asterisks correspond to cryo-EM structures. Abbreviations: ALP, alprazolam; ATR, all-*trans*-retinal; BCC, bicuculline; CHS, cholesterol hemisuccinate; DAMGO, [D-Ala^2, N-MePhe^4, Gly-ol]-enkephalin; DDM, *n*-dodecyl β-D-maltoside; DDTM, *n*-dodecyl 1-thio-β-maltoside; DMNG, decyl maltose neopentyl glycol; DZP, diazepam; EMDB, Electron Microscopy Data Bank; FUB, MDMB-fubinaca; GABA, γ-aminobutyric acid; $GABA_AR$, γ-aminobutyric acid A receptor; GDN, glyco-diosgenin; GPCR, G protein–coupled receptor; LMNG, lauryl maltose neopentyl glycol; NA, not applicable; NAM, negative allosteric modulator; NECA, (2*S*,3*S*,4*R*,5*R*)-5-(6-amino-9H-purin-9-yl)-*N*-ethyl-3,4-dihydroxytetrahydrofuran-2-carboxamide; PAM, positive allosteric modulator; PDB, Protein Data Bank; PS, pregnenolone sulfate; PTX, picrotoxinin; Res^n, resolution; THDOC, tetrahydrodeoxycorticosterone.

triggers closure of the pocket and an asymmetric counterclockwise rotation of the ECD (when looking down the pore axis from the extracellular side), leaving one GABA binding site looser than the other [potentially explaining the difference in affinity between the two neurotransmitter sites (101)]. The conformational change in the ECD is transduced to the TMD through the subunit-specific M2–M3 loop, which opens the channel pore.

Cryo-EM has brought significant insights into the binding mode and molecular mechanism of receptor regulation of currently used therapeutics (**Figure 2**). Benzodiazepines are positive allosteric modulators and bind at the α+/γ− site. They improve the connectivity between subunits and aid in transmitting the conformational change across all chains upon binding of GABA. An additional binding site for diazepam was found at the β+/γ− site at the TMD level, which further acts as a positive allosteric modulator and explains the biphasic potentiation produced by increasing concentrations of diazepam (101). Bicuculline is a competitive antagonist and binds at the β+/α− sites where its bulkiness prevents full closure of the pocket, thus locking the receptor in a closed state. Flumazenil is an antagonist of benzodiazepines and is clinically used for the treatment of benzodiazepine overdose. It binds to the α+/γ− site but interacts mostly with the α subunit, unlike a positive allosteric modulator. Picrotoxin acts as a pore blocker and binds at the channel between M2 2′ and 9′ rings and also stabilizes the resting/closed states, diminishing the affinity for agonists.

In the last year, cryo-EM structures of $GABA_ARs$ have added significantly to our understanding of how drugs bind and why they work as either agonists or antagonists. More than three times as many structures of $GABA_ARs$ have been determined by cryo-EM than by X-ray crystallography, with the resolution of the structures in a similar range for both techniques. When comparing the resolutions and quality of the densities for drugs and proteins, it can be appreciated that the quality of experimental density is similar for cryo-EM and X-ray crystallography (**Figures 2** and **3*c***). However, cryo-EM has crucial advantages over X-ray crystallography for the $GABA_ARs$ because structures can be determined for full-length native receptors in a lipid bilayer within a nanodisc. This yields structures with physiologically relevant conformations, unlike the structures in

detergent solutions where the pore is collapsed (**Figure 3*a***). In addition, cryo-EM structures of the α1β3γ2L receptor identified phosphatidylinositol-4,5-bisphosphate [PtdIns(4,5)P_2, or PIP_2] (45, 46), bound at a TMD site formed by α1M3, α1M4, and the loop between α1M1-M2 (**Figure 3*b***), although the physiological relevance of this is unclear. Cryo-EM structures have also identified the partial structure of *N*-glycans on Asn111 of the α1 subunit, which are present in the receptor vestibule. The *N*-glycans have been hypothesized to control receptor assembly, since their bulky nature would only allow incorporation of one or two α1 subunits per receptor (**Figure 3*d***).

One technical hurdle that had to be overcome for cryo-EM structural determination of heteromeric $GABA_A$Rs was how to break the pseudo-fivefold symmetry of the channels during structure determination. Initially, particles are aligned using predominantly low-resolution information, but this cannot distinguish between the different subunits in, for example, the α1β3γ2L receptor. Binding specific antibodies, such as camelid nanobodies (45, 46) or murine F_{ab}s (99, 100), to different receptor subunits has solved this problem. Antibody binding was also essential to gain random orientations of the particles on the cryo-EM grids for $GABA_A$R reconstituted into nanodiscs, which is a prerequisite for structural determination.

CASE STUDY 2: G PROTEIN–COUPLED RECEPTORS

Introduction to G Protein–Coupled Receptors and Their Pharmacology

GPCRs sense a variety of extracellular stimuli (from neurotransmitters to light) and transduce the information to the interior of the cell by coupling to and activating heterotrimeric G proteins and β-arrestins (102–104). GPCRs have a well-established therapeutic value and are the target for 34% of US Food and Drug Administration–approved drugs (105). GPCRs can be divided into six different families based on sequence and functional similarity: These include classes A (rhodopsin-like), B (secretin-like), C (metabotropic glutamate receptors), D (fungal mating pheromone receptors), E (cAMP receptors), and F (Frizzled/smoothened receptors), with class A being the largest family. In a typical functional cycle of signal transduction, receptors in an inactive state bind to extracellular chemical signals (agonists), which increases the probability of transitions to an active state, and then couple and activate heterotrimeric G proteins and β-arrestins. Extensive developments in technology and biochemical tools have facilitated the structure determination of over 50 different GPCRs bound to different ligands by X-ray crystallography (over 280 GPCR structures have been determined in total). However, virtually all of these structures are of GPCRs in an inactive or intermediate state, with only three structures coupled to a G protein (106–108). Using cryo-EM makes it possible to determine structures of GPCRs coupled to G proteins, which was very difficult using X-ray crystallography.

From Crystal to Cryo-Electron Microscopy Structures of G Protein–Coupled Receptors

For a long time, GPCRs were recalcitrant to structural determination by X-ray crystallography. Crystallization and structural determination of GPCRs required the development of biochemical and technological tools (109) such as the incorporation of fusion proteins (110), improved detergents (111), use of the lipidic cubic phase (112), and the development of synchrotron microfocus beamlines (113). This generated a wide range of structural information, albeit mainly of class A GPCRs in inactive states bound to antagonists or inverse agonists (114). A few structures of GPCRs bound to agonists have also been solved (115), but GPCRs do not adopt a fully active conformation until they are bound to their intracellular transducer partner. Strategies to trap fully active states included the use of peptides mimicking the C-terminal α-helix (α5) of the

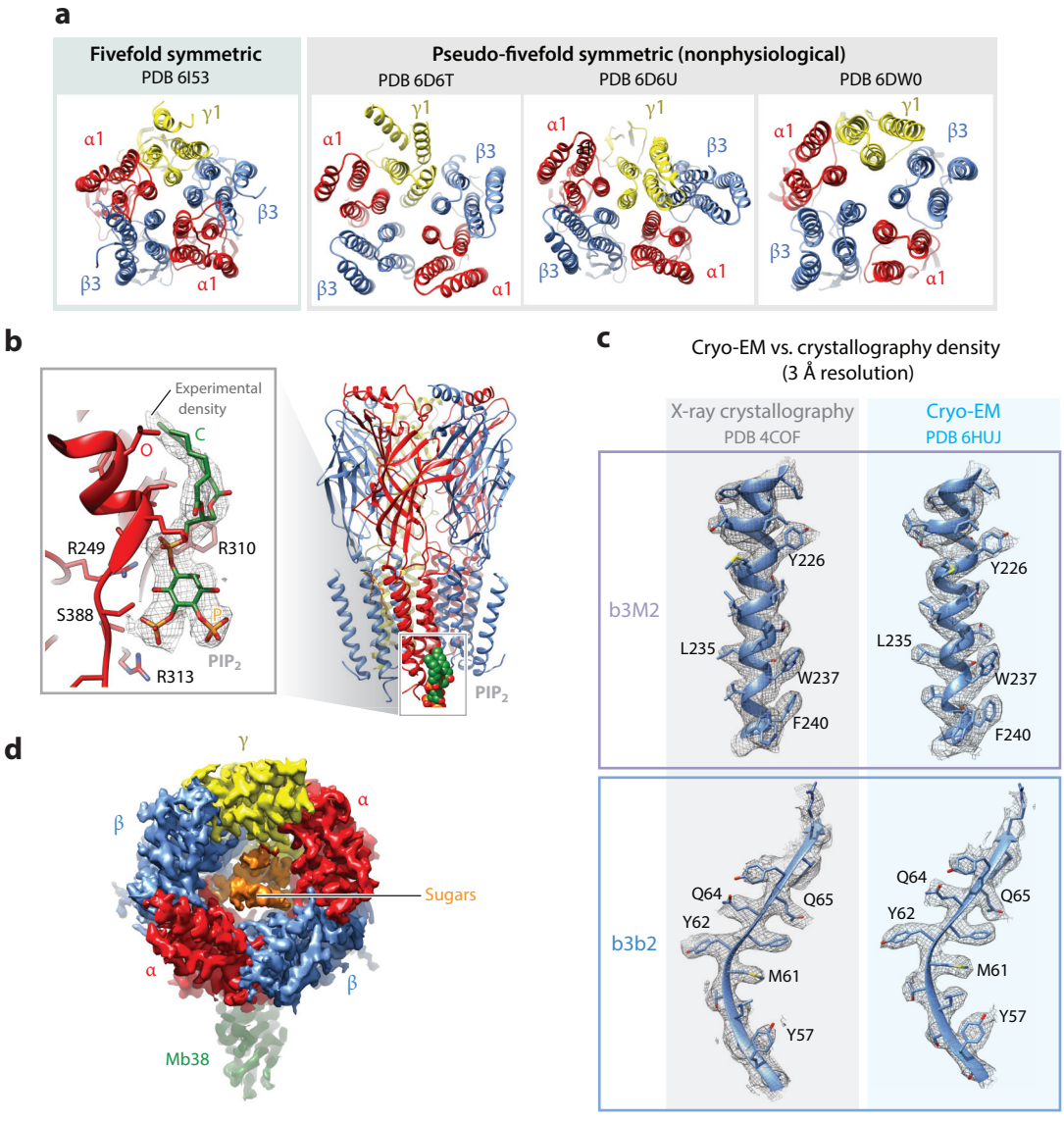

Figure 3

Cryo-electron microscopy (cryo-EM) versus X-ray crystallography in γ-aminobutyric acid A receptors ($GABA_AR$s). (*a*) Intracellular views of the heteromeric structures containing a γ subunit (α, *red*; β, *blue*, γ, *yellow*). (*b*) The PIP_2 molecule bound to the $GABA_AR$ is shown as a space-filling model (C, *green*; O, *red*; P, *orange*), with the inset showing experimental density (*gray mesh*) surrounding PIP_2, which is depicted as sticks. (*c*) Comparison of crystallography electron density (PDB 4COF) and cryo-EM density (EMDB 0279) for two secondary structure elements of the β3 subunit. Both maps are at 3 Å resolution. Density is represented as gray mesh and the protein diagram is colored light blue. (*d*) Cryo-EM density (EMDB 0279) of the $GABA_AR$ viewed from the extracellular surface (α, *red*; β, *blue*, γ, *yellow*), including the Megabody 38 (Mb38, *green*) and the $GABA_AR$ intra-vestibule glycosylation (*orange*).

G protein α-subunit (116), conformation-specific intracellular nanobodies (117), and mini–G proteins (106, 108). There is only a single crystal structure of a GPCR, the β_2-adrenoceptor, in complex with a G_s heterotrimer stabilized by a nanobody (Nb35) (107). In the past two years, significant progress has occurred with the structure determination of GPCRs coupled to different heterotrimeric G proteins (G_s, G_i, G_O) and active-state structures of class A, B, and C GPCRs. In addition, the mechanism of receptor activity–modifying proteins (RAMPs) in modulating receptor pharmacology has been uncovered as well as how HIV binds to GPCRs to promote viral entry into host cells. A summary of the structures with the relevant references is shown in **Table 1**.

GPCRs couple to and activate specific heterotrimeric G proteins that are composed of an α, β, and γ subunit. The α-subunit mostly determines coupling specificity, and there are 16 different Gα genes encoded by the human genome that are grouped into four different families (G_s, $G_{i/o}$, $G_{q/11}$, $G_{12/13}$). Each Gα family activates/inhibits different intracellular signaling cascades. Until recently, information was scarce on the selectivity code by which GPCR and G proteins discriminate for each other. The structures of several drug–GPCR–G protein complexes have been determined by cryo-EM, including four G_s-coupled receptors [CTR (57, 118), GLP-1 receptor (56, 119), CGRP receptor (58), and A_{2A} receptor (53)], four G_i-coupled receptors [Rhodopsin (120), μOR (121), CB_1 receptor (122), and A_1 receptor (55)], and one G_o-coupled receptor [the serotonin 5-HT_{1B} receptor (54)]. In-depth analysis of the different GPCR–G protein interfaces suggests that there is no amino acid sequence barcode that determines coupling specificity (16, 17). There are sequence-conserved residues at the C-terminal end of the α-subunit that make conserved interactions with the receptors. The extent of outward movement of the intracellular part of TM6, which is a hallmark in the activation of GPCRs, varies between G_s- and $G_{i/o}$-coupled receptors, with $G_{i/o}$ having a smaller movement than G_s (**Figure 4*a***). This correlates with the bulkiness of the α5 helix of G_s compared to $G_{i/o}$. The surface of receptor–G protein interaction seems to be larger for G_s than $G_{i/o}$, with $G_{i/o}$ normally losing the interaction with the receptor ICL2. However, there are no hard and fast rules for any of these features, and there seem to be numerous outliers. Although conserved interactions are seen for each G protein, it seems that different receptors have arrived at slightly different solutions for binding the same G protein, and further structures are needed to understand GPCR–G protein selectivity. Furthermore, receptors do not always have strict preferences for G proteins and can be promiscuous with different stringencies for different G proteins. Such versatility will make understanding GPCR–G protein selectivity nontrivial.

Three of the G_s-coupled structures contain GPCRs belonging to class B receptors, i.e., CTR, GLP-1R, and the CGRP receptor. These are the first class B GPCR structures in the active state bound to G proteins that have been determined and show novel features when compared to class A GPCRs. Class B GPCRs bind peptide agonists using a large extracellular N-terminal domain. The ligand-binding pocket is open much wider than in class A GPCRs. Upon activation, there is a very sharp kink in helix 6, which results in a pronounced outward movement of the intracellular ends of helices 6 and 7 when compared to the class A receptors. Class B GPCRs seem to have a characteristic long helix 8 that contacts the β-subunit of the G protein, which is not the case for class A receptors (**Figure 4*b***). The CGRP receptor is a heterodimer formed by the calcitonin receptor–like receptor (CLR) and a RAMP (123). RAMPs change the agonist selectivity of receptors, and the cryo-EM structure shows that the RAMP does not interact with the ligand. The RAMP sits at the interface between transmembrane helices 3, 4, and 5 of the CLR and modifies the agonist selectivity by allosteric stabilization of the receptor in a specific conformation (**Figure 4*c***).

Another breakthrough in the structural investigation of GPCRs is the structure determination of the dimeric class C metabotropic glutamate receptor 5 (mGluR5) (124). mGluRs are obligate

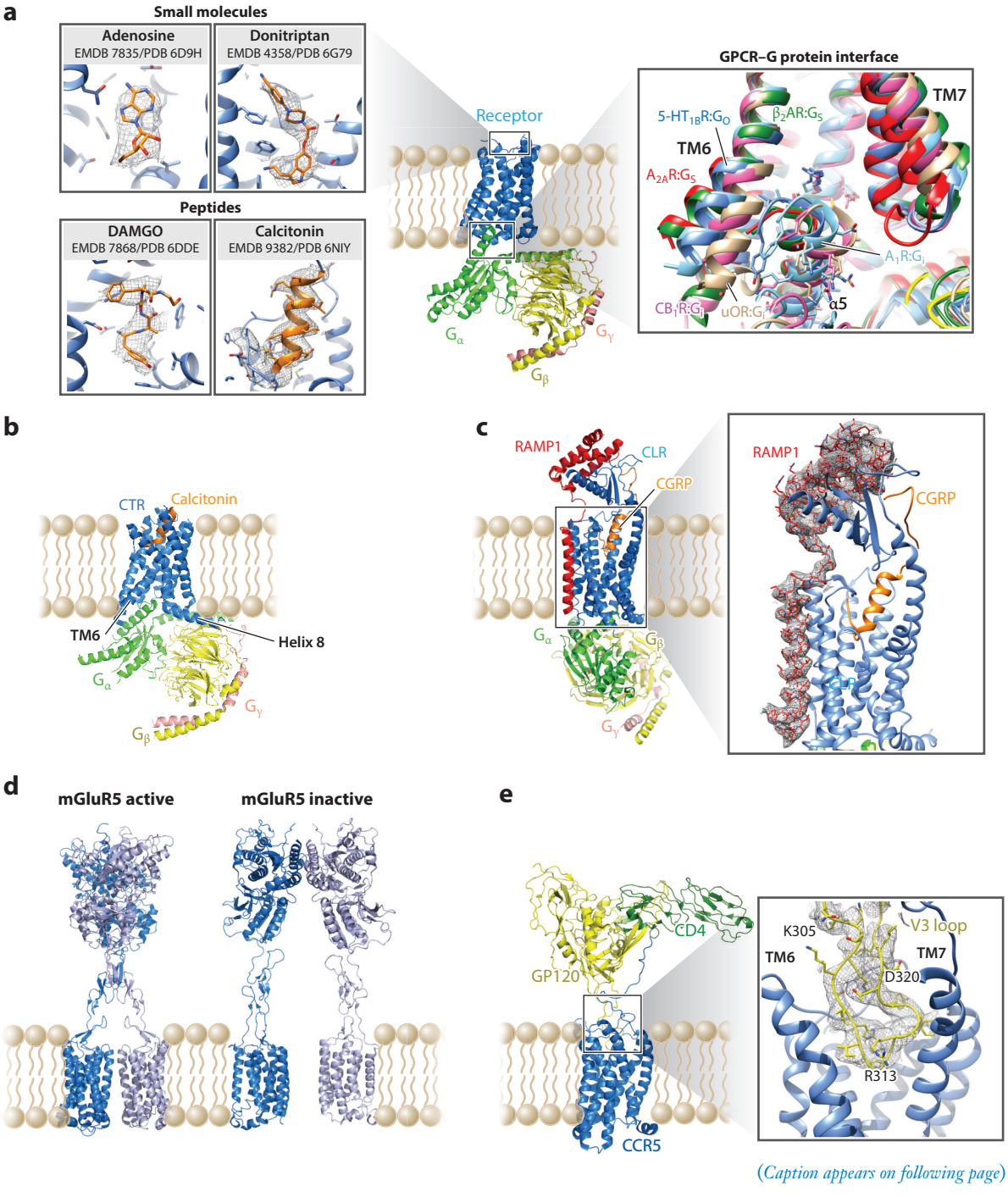

(Caption appears on following page)

Figure 4 (*Figure appears on preceding page*)

Cryo-EM of GPCR–G protein complexes. For all panels, cryo-EM density is shown as gray mesh, and the protein is depicted with key side chains as sticks. (*a*) GPCR–G protein complexes highlighting (*left*) ligands of different natures at the ligand-binding pocket and (*right*) features of the GPCR–G protein interface. Ligands are depicted as sticks with carbon atoms in orange. (*b*) Class B GPCR with the CTR as an example. (*c*) The CGRP receptor with RAMP (*red*). (*d*) Two conformations corresponding to the apo- and agonist-bound metabotropic GluR5. (*e*) The structure of the CCR5–GP120–CD4 complex, with insight into the interaction of GP120 at the CCR5 ligand-binding pocket. Abbreviations: cryo-EM, cryo-electron microscopy; CTR, calcitonin receptor; CGRP, calcitonin gene–related peptide receptor; GPCR, G protein–coupled receptor; RAMP, receptor activity–modifying protein; mGluR5, metabotropic glutamate receptor 5; CCR5, C-C chemokine receptor 5; CB_1R, cannabinoid receptor 1; $5\text{-}HT_{1B}R$, serotonin $5\text{-}HT_{1B}$ receptor; $A_{2A}R$, adenosine A_{2A} receptor; μOR, μ opioid receptor; A_1R, adenosine A_1 receptor; β_2AR, β_2 adrenergic receptor.

dimers and contain a TMD and an ECD connected by a cysteine-rich domain (**Figure 4*d***). Crystal structures of the TMD (125, 126) and the ECD (127) were previously available, but the full-length structure determined by cryo-EM was necessary to explain how the signal is transduced from the ECD, which binds glutamate, to the TMD (**Figure 4*d***).

Lastly, a recent structure was reported of the chemokine receptor CCR5 in complex with GP120 and CD4—a complex responsible for viral and host membrane fusion in HIV infection (128) (**Figure 4*e***). HIV entry into host cells is mediated by GP160 (cleaved into GP120 and GP41), which binds to CD4 and a coreceptor (i.e., CCR5 or CXCR4). GP120 binding to chemokine receptors is essential for viral entry, and its role has been elucidated through the determination of the cryo-EM structure of the CCR5–GP120–CD4 complex. The V3 loop of GP120 occupies the ligand-binding pocket of CCR5, which is in an inactive conformation. The structure of the complex suggests new potential routes to improve anti-HIV therapeutics, such as modifications of the currently used drug maraviroc to inhibit viral entry. Given the shape and flexibility of the CCR5–GP120–CD4 complex shown by cryo-EM, it is difficult to imagine how well-diffracting crystals could be produced for X-ray crystallography.

THE USE OF ELECTRON CRYO-MICROSCOPY FOR STRUCTURE-BASED DRUG DISCOVERY: $GABA_A$ RECEPTORS AND G PROTEIN–COUPLED RECEPTORS

Structural determination by cryo-EM is far from the high-throughput capabilities of X-ray crystallography, but it can still provide essential information intractable to X-ray crystallography. SSBD benefits from different levels of structural information. First, any structure of the protein target is potentially valuable, as it suggests possible mechanisms and can also be used for screening computational libraries of compounds aimed at trapping a specific functional state. The use of membrane protein cryo-EM structures has already been used in deciphering the binding modes of small-molecule therapeutics (129). The next level of information is the structure of the first drug–protein complex, which experimentally identifies a ligand-binding pocket and identifies interactions, geometry, and properties of the pocket. This information greatly improves the efficiency of further searches in the chemical space of the ligands. The last step is when a series of drug–protein complexes with slight variations in ligand chemistry can be produced to fully understanding the structure–activity relationship. At this level, one needs to be able to produce tens or even hundreds of structures of the protein target with different molecules. Although cryo-EM cannot yet provide so many structures in a short span of time, it is an invaluable tool that can provide initial structures of the protein targets and the first structures of drug–receptor complexes. This is clearly shown in the case of both $GABA_AR$s and GPCRs, where cryo-EM has allowed the structure determination of novel receptors, different functional states, and receptors bound to a variety of small-molecule therapeutics. In the case of $GABA_AR$s, it also provides

physiological conformations of heteromeric channels. Moreover, although higher resolution is desirable for SBDD, the cryo-EM maps were of similar quality when compared to X-ray crystallography maps and allowed unambiguous refinement of the position and orientation of the small molecules. For GPCRs, the structures of novel receptors were determined, and they can now be used for computational drug design. However, the resolution of structures was worse than for $GABA_A$Rs, probably due to the small size of the complexes.

In terms of throughput, GPCRs required, on average, thousands of well-populated micrographs, generally requiring more than four days of data collection. This generates large amounts of data that also require longer times for computation and data processing. Therefore, structure determination of GPCRs by cryo-EM is most suited to producing the first structure of a new drug target and selected structures bound to key lead compounds rather than producing large numbers of structures. However, structures generated for $GABA_A$Rs were solved using less than 1,000 micrographs, which is equivalent to about a day of data collection. The number of images and the low number of particles in the final models (30,000–60,000 particles) allow fast processing from particle picking to map refinement, where the map is produced within 24–48 h. Cryo-EM of $GABA_A$Rs is thus the first example where there is a possibility of SBDD and where two or three structures might be determined per week, provided there is access to the appropriate resources.

CONCLUSIONS AND FUTURE PERSPECTIVES

Cryo-EM has recently undergone a significant revolution, and it is now possible to determine structures that were thought impossible even just a few years ago. This revolution has not stopped, and further significant improvements over the coming years are anticipated. Direct electron detectors will collect more data faster as they increase in area and data handling speeds are improved. They are still not 100% efficient in detecting every electron at all spatial frequencies, and improvements in this area will have a significant impact on the quality of data collected. There are also improvements in progress in the electron microscope itself, which improve the coherence of the electron beam and phase plate technology (130). In addition, significant improvements to grid preparation are possible to prevent preferential sample orientation and sample denaturation (131). Finally, it is inevitable that further improvements will be made in the computational aspects of data processing and structural determination. Discussions of SBDD on membrane proteins using cryo-EM are thus not so much about whether it will ever be possible but when it will happen. For the $GABA_A$Rs, it can be argued that if sufficient resources are available, then SBDD is a reality. For GPCRs, where 5–10 times more data and processing time are required, further advances in technology are required. However, it is notable that some GPCR complexes are far more tractable for structure determination than others, which is probably a reflection of the stability of the complexes. So, as with X-ray crystallography, the choice of the target has a significant impact on the probability of success. In addition, good biochemistry is essential to make an optimally stable sample suitable for cryo-EM.

DISCLOSURE STATEMENT

C.G.T. is a shareholder, consultant, and member of the Scientific Advisory Board of Heptares Therapeutics.

ACKNOWLEDGMENTS

Research on GPCR complexes in C.G.T.'s laboratory is funded by Heptares Therapeutics (to J.G.-N.), a European Research Council grant (EMPSI 339995), and core funding from the Medical Research Council (MRC U105197215).

LITERATURE CITED

1. Almen MS, Nordstrom KJ, Fredriksson R, Schioth HB. 2009. Mapping the human membrane proteome: A majority of the human membrane proteins can be classified according to function and evolutionary origin. *BMC Biol.* 7:50
2. Lander ES, Linton LM, Birren B, Nusbaum C, Zody MC, et al. 2001. Initial sequencing and analysis of the human genome. *Nature* 409:860–921
3. Overington JP, Al-Lazikani B, Hopkins AL. 2006. How many drug targets are there? *Nat. Rev. Drug Discov.* 5:993–96
4. Sledz P, Caflisch A. 2018. Protein structure-based drug design: from docking to molecular dynamics. *Curr. Opin. Struct. Biol.* 48:93–102
5. Bai XC, Yan C, Yang G, Lu P, Ma D, et al. 2015. An atomic structure of human γ-secretase. *Nature* 525:212–17
6. Bai XC, Rajendra E, Yang G, Shi Y, Scheres SH. 2015. Sampling the conformational space of the catalytic subunit of human γ-secretase. *eLife* 4:e11182
7. Liu F, Zhang Z, Csanady L, Gadsby DC, Chen J. 2017. Molecular structure of the human CFTR ion channel. *Cell* 169:85–95.e8
8. Zhang Z, Chen J. 2016. Atomic structure of the cystic fibrosis transmembrane conductance regulator. *Cell* 167:1586–97.e9
9. Wang W, MacKinnon R. 2017. Cryo-EM structure of the open human ether-a-go-go-related K^+ channel hERG. *Cell* 169:422–30.e10
10. Shen H, Liu D, Wu K, Lei J, Yan N. 2019. Structures of human $Na_v1.7$ channel in complex with auxiliary subunits and animal toxins. *Science* 363:1303–8
11. Vandenberg JI, Perozo E, Allen TW. 2017. Towards a structural view of drug binding to hERG K^+ channels. *Trends Pharmacol. Sci.* 38:899–907
12. Lau C, Hunter MJ, Stewart A, Perozo E, Vandenberg JI. 2018. Never at rest: insights into the conformational dynamics of ion channels from cryo-electron microscopy. *J. Physiol.* 596:1107–19
13. Shimada I, Ueda T, Kofuku Y, Eddy MT, Wuthrich K. 2019. GPCR drug discovery: integrating solution NMR data with crystal and cryo-EM structures. *Nat. Rev. Drug Discov.* 18:59–82
14. Zhou XE, Melcher K, Xu HE. 2019. Structural biology of G protein-coupled receptor signaling complexes. *Protein Sci.* 28:487–501
15. Thal DM, Glukhova A, Sexton PM, Christopoulos A. 2018. Structural insights into G-protein-coupled receptor allostery. *Nature* 559:45–53
16. Glukhova A, Draper-Joyce CJ, Sunahara RK, Arthur Christopoulos, Wotten D, Sexton PM. 2018. Rules of engagement: GPCRs and G proteins. *ACS Pharmacol. Trans. Sci.* 1:73–142
17. García-Nafría J, Tate CG. 2019. Cryo-EM structures of GPCRs coupled to G_s, G_i and G_o. *Mol. Cell. Endocrinol.* 488:1–13
18. Vinothkumar KR, Henderson R. 2016. Single particle electron cryomicroscopy: trends, issues and future perspective. *Q. Rev. Biophys.* 49:e13
19. Passmore LA, Russo CJ. 2016. Specimen preparation for high-resolution cryo-EM. *Methods Enzymol.* 579:51–86
20. Cheng Y. 2015. Single-particle cryo-EM at crystallographic resolution. *Cell* 161:450–57
21. Fernandez-Leiro R, Scheres SH. 2016. Unravelling biological macromolecules with cryo-electron microscopy. *Nature* 537:339–46
22. Renaud JP, Chari A, Ciferri C, Liu WT, Remigy HW, et al. 2018. Cryo-EM in drug discovery: achievements, limitations and prospects. *Nat. Rev. Drug Discov.* 17:471–92
23. Scapin G, Potter CS, Carragher B. 2018. Cryo-EM for small molecules discovery, design, understanding, and application. *Cell Chem. Biol.* 25:1318–25
24. Merino F, Raunser S. 2017. Electron cryo-microscopy as a tool for structure-based drug development. *Angew. Chem. Int. Ed.* 56:2846–60
25. Boland A, Chang L, Barford D. 2017. The potential of cryo-electron microscopy for structure-based drug design. *Essays Biochem.* 61:543–60

26. Subramaniam S, Earl LA, Falconieri V, Milne JL, Egelman EH. 2016. Resolution advances in cryo-EM enable application to drug discovery. *Curr. Opin. Struct. Biol.* 41:194–202
27. Kuhlbrandt W. 2014. The resolution revolution. *Science* 343:1443–44
28. Tate CG. 2010. Practical considerations of membrane protein instability during purification and crystallisation. *Methods Mol. Biol.* 601:187–203
29. Liao M, Cao E, Julius D, Cheng Y. 2014. Single particle electron cryo-microscopy of a mammalian ion channel. *Curr. Opin. Struct. Biol.* 27:1–7
30. Campbell MG, Cheng A, Brilot AF, Moeller A, Lyumkis D, et al. 2012. Movies of ice-embedded particles enhance resolution in electron cryo-microscopy. *Structure* 20:1823–28
31. Scheres SH. 2014. Beam-induced motion correction for sub-megadalton cryo-EM particles. *eLife* 3:e03665
32. Ripstein ZA, Rubinstein JL. 2016. Processing of cryo-EM movie data. *Methods Enzymol.* 579:103–24
33. Zivanov J, Nakane T, Scheres SHW. 2019. A Bayesian approach to beam-induced motion correction in cryo-EM single-particle analysis. *IUCrJ* 6(1):5–17
34. Scheres SHW. 2012. RELION: implementation of a Bayesian approach to cryo-EM structure determination. *J. Struct. Biol.* 180:519–30
35. Zivanov J, Nakane T, Forsberg BO, Kimanius D, Hagen WJ, et al. 2018. New tools for automated high-resolution cryo-EM structure determination in RELION-3. *eLife* 7:e42166
36. Grant T, Rohou A, Grigorieff N. 2018. *cis*TEM, user-friendly software for single-particle image processing. *eLife* 7:e35383
37. Grigorieff N. 2016. Frealign: an exploratory tool for single-particle cryo-EM. *Methods Enzymol.* 579:191–226
38. Russo CJ, Henderson R. 2018. Ewald sphere correction using a single side-band image processing algorithm. *Ultramicroscopy* 187:26–33
39. Glaeser RM, Typke D, Tiemeijer PC, Pulokas J, Cheng A. 2011. Precise beam-tilt alignment and collimation are required to minimize the phase error associated with coma in high-resolution cryo-EM. *J. Struct. Biol.* 174:1–10
40. McMullan G, Faruqi AR, Henderson R. 2016. Direct electron detectors. *Methods Enzymol.* 579:1–17
41. Bai XC, McMullan G, Scheres SHW. 2015. How cryo-EM is revolutionizing structural biology. *Trends Biochem. Sci.* 40:49–57
42. Taylor KA, Glaeser RM. 2008. Retrospective on the early development of cryoelectron microscopy of macromolecules and a prospective on opportunities for the future. *J. Struct. Biol.* 163:214–23
43. Glaeser RM, Han BG. 2017. Opinion: hazards faced by macromolecules when confined to thin aqueous films. *Biophys. Rep.* 3:1–7
44. Noble AJ, Wei H, Dandey VP, Zhang Z, Tan YZ, et al. 2018. Reducing effects of particle adsorption to the air-water interface in cryo-EM. *Nat. Methods* 15:793–95
45. Masiulis S, Desai R, Uchanski T, Serna Martin I, Laverty D, et al. 2019. $GABA_A$ receptor signalling mechanisms revealed by structural pharmacology. *Nature* 565:454–59
46. Laverty D, Desai R, Uchanski T, Masiulis S, Stec WJ, et al. 2019. Cryo-EM structure of the human $\alpha1\beta3\gamma2$ $GABA_A$ receptor in a lipid bilayer. *Nature* 565:516–20
47. Russo CJ, Passmore LA. 2016. Progress towards an optimal specimen support for electron cryomicroscopy. *Curr. Opin. Struct. Biol.* 37:81–89
48. Danev R, Buijsse B, Khoshouei M, Plitzko JM, Baumeister W. 2014. Volta potential phase plate for in-focus phase contrast transmission electron microscopy. *PNAS* 111:15635–40
49. Khoshouei M, Radjainia M, Baumeister W, Danev R. 2017. Cryo-EM structure of haemoglobin at 3.2 Å determined with the Volta phase plate. *Nat. Commun.* 8:16099
50. Danev R, Tegunov D, Baumeister W. 2017. Using the Volta phase plate with defocus for cryo-EM single particle analysis. *eLife* 6:e23006
51. Danev R, Baumeister W. 2016. Cryo-EM single particle analysis with the Volta phase plate. *eLife* 5:e13046
52. von Loeffelholz O, Papai G, Danev R, Myasnikov AG, Natchiar SK, et al. 2018. Volta phase plate data collection facilitates image processing and cryo-EM structure determination. *J. Struct. Biol.* 202:191–99

53. García-Nafría J, Lee Y, Bai X, Carpenter B, Tate CG. 2018. Cryo-EM structure of the adenosine A_{2A} receptor coupled to an engineered heterotrimeric G protein. *eLife* 7:e35946
54. García-Nafría J, Nehme R, Edwards PC, Tate CG. 2018. Cryo-EM structure of the serotonin 5-HT_{1B} receptor coupled to heterotrimeric G_o. *Nature* 558:620–23
55. Draper-Joyce CJ, Khoshouei M, Thal DM, Liang YL, Nguyen ATN, et al. 2018. Structure of the adenosine-bound human adenosine A1 receptor-G_i complex. *Nature* 558:559–63
56. Liang YL, Khoshouei M, Glukhova A, Furness SGB, Zhao P, et al. 2018. Phase-plate cryo-EM structure of a biased agonist-bound human GLP-1 receptor-Gs complex. *Nature* 555:121–25
57. Liang YL, Khoshouei M, Radjainia M, Zhang Y, Glukhova A, et al. 2017. Phase-plate cryo-EM structure of a class B GPCR–G-protein complex. *Nature* 546:118–23
58. Liang YL, Khoshouei M, Deganutti G, Glukhova A, Koole C, et al. 2018. Cryo-EM structure of the active, G_s-protein complexed, human CGRP receptor. *Nature* 561:492–97
59. Herzik MA Jr., Wu M, Lander GC. 2019. High-resolution structure determination of sub-100 kDa complexes using conventional cryo-EM. *Nat. Commun.* 10:1032
60. Strege A, Carpenter B, Edwards PC, Tate CG. 2017. Strategy for the thermostabilization of an agonist-bound GPCR coupled to a G protein. *Methods Enzymol.* 594:243–64
61. Magnani F, Serrano-Vega MJ, Shibata Y, Abdul-Hussein S, Lebon G, et al. 2016. A mutagenesis and screening strategy to generate optimally thermostabilized membrane proteins for structural studies. *Nat. Protoc.* 11:1554–71
62. Robertson N, Jazayeri A, Errey J, Baig A, Hurrell E, et al. 2011. The properties of thermostabilised G protein-coupled receptors (StaRs) and their use in drug discovery. *Neuropharmacology* 60:36–44
63. Merk A, Bartesaghi A, Banerjee S, Falconieri V, Rao P, et al. 2016. Breaking cryo-EM resolution barriers to facilitate drug discovery. *Cell* 165:1698–707
64. Li H, O'Donoghue AJ, van der Linden WA, Xie SC, Yoo E, et al. 2016. Structure- and function-based design of *Plasmodium*-selective proteasome inhibitors. *Nature* 530:233–36
65. Morris EP, da Fonseca PCA. 2017. High-resolution cryo-EM proteasome structures in drug development. *Acta Crystallogr. D Struct. Biol.* 73:522–33
66. Liao M, Cao E, Julius D, Cheng Y. 2013. Structure of the TRPV1 ion channel determined by electron cryo-microscopy. *Nature* 504:107–12
67. Gao Y, Cao E, Julius D, Cheng Y. 2016. TRPV1 structures in nanodiscs reveal mechanisms of ligand and lipid action. *Nature* 534:347–51
68. Congreve M, Oswald C, Marshall FH. 2017. Applying structure-based drug design approaches to allosteric modulators of GPCRs. *Trends Pharmacol. Sci.* 38:837–47
69. Congreve M, Dias JM, Marshall FH. 2014. Structure-based drug design for G protein-coupled receptors. *Prog. Med. Chem.* 53:1–63
70. Rucktooa P, Cheng RKY, Segala E, Geng T, Errey JC, et al. 2018. Towards high throughput GPCR crystallography: *in meso* soaking of adenosine A_{2A} receptor crystals. *Sci. Rep.* 8:41
71. Collins PM, Douangamath A, Talon R, Dias A, Brandao-Neto J, et al. 2018. Achieving a good crystal system for crystallographic X-ray fragment screening. *Methods Enzymol.* 610:251–64
72. Kimanius D, Forsberg BO, Scheres SH, Lindahl E. 2016. Accelerated cryo-EM structure determination with parallelisation using GPUs in RELION-2. *eLife* 5:e18722
73. Heymann JB. 2018. Map challenge assessment: fair comparison of single particle cryoEM reconstructions. *J. Struct. Biol.* 204:360–67
74. Gomez-Blanco J, de la Rosa-Trevin JM, Marabini R, Del Cano L, Jimenez A, et al. 2018. Using *Scipion* for stream image processing at Cryo-EM facilities. *J. Struct. Biol.* 204:457–63
75. Terwilliger TC, Adams PD, Afonine PV, Sobolev OV. 2018. A fully automatic method yielding initial models from high-resolution cryo-electron microscopy maps. *Nat. Methods* 15:905–8
76. Mendez JH, Stagg SM. 2018. Assessing the quality of single particle reconstructions by atomic model building. *J. Struct. Biol.* 204:276–82
77. Sieghart W. 1995. Structure and pharmacology of γ-aminobutyric $acid_A$ receptor subtypes. *Pharmacol. Rev.* 47:181–234

78. Sigel E, Steinmann ME. 2012. Structure, function, and modulation of $GABA_A$ receptors. *J. Biol. Chem.* 287:40224–31
79. Farrant M, Nusser Z. 2005. Variations on an inhibitory theme: phasic and tonic activation of $GABA_A$ receptors. *Nat. Rev. Neurosci.* 6:215–29
80. Rudolph U, Mohler H. 2014. $GABA_A$ receptor subtypes: therapeutic potential in Down syndrome, affective disorders, schizophrenia, and autism. *Annu. Rev. Pharmacol. Toxicol.* 54:483–507
81. Belelli D, Lambert JJ. 2005. Neurosteroids: endogenous regulators of the $GABA_A$ receptor. *Nat. Rev. Neurosci.* 6:565–75
82. Hosie AM, Wilkins ME, da Silva HM, Smart TG. 2006. Endogenous neurosteroids regulate $GABA_A$ receptors through two discrete transmembrane sites. *Nature* 444:486–89
83. Chua HC, Chebib M. 2017. $GABA_A$ receptors and the diversity in their structure and pharmacology. *Adv. Pharmacol.* 79:1–34
84. Braat S, Kooy RF. 2015. The $GABA_A$ receptor as a therapeutic target for neurodevelopmental disorders. *Neuron* 86:1119–30
85. Franks NP. 2008. General anaesthesia: from molecular targets to neuronal pathways of sleep and arousal. *Nat. Rev. Neurosci.* 9:370–86
86. Rudolph U, Knoflach F. 2011. Beyond classical benzodiazepines: novel therapeutic potential of $GABA_A$ receptor subtypes. *Nat. Rev. Drug Discov.* 10:685–97
87. Thompson SA, Whiting PJ, Wafford KA. 1996. Barbiturate interactions at the human $GABA_A$ receptor: dependence on receptor subunit combination. *Br. J. Pharmacol.* 117:521–27
88. Wallner M, Hanchar HJ, Olsen RW. 2003. Ethanol enhances $\alpha4\beta3\delta$ and $\alpha6\beta3\delta$ γ-aminobutyric acid type A receptors at low concentrations known to affect humans. *PNAS* 100:15218–23
89. Simon J, Wakimoto H, Fujita N, Lalande M, Barnard EA. 2004. Analysis of the set of $GABA_A$ receptor genes in the human genome. *J. Biol. Chem.* 279:41422–35
90. Olsen RW, Sieghart W. 2008. International Union of Pharmacology. LXX. Subtypes of γ-aminobutyric $acid_A$ receptors: classification on the basis of subunit composition, pharmacology, and function. Update. *Pharmacol. Rev.* 60:243–60
91. Knoflach F, Benke D, Wang Y, Scheurer L, Luddens H, et al. 1996. Pharmacological modulation of the diazepam-insensitive recombinant gamma-aminobutyric acidA receptors alpha 4 beta 2 gamma 2 and alpha 6 beta 2 gamma 2. *Mol. Pharmacol.* 50:1253–61
92. Tan KR, Rudolph U, Luscher C. 2011. Hooked on benzodiazepines: $GABA_A$ receptor subtypes and addiction. *Trends Neurosci.* 34:188–97
93. Miller PS, Smart TG. 2010. Binding, activation and modulation of Cys-loop receptors. *Trends Pharmacol. Sci.* 31:161–74
94. Miller PS, Aricescu AR. 2014. Crystal structure of a human $GABA_A$ receptor. *Nature* 512:270–75
95. Laverty D, Thomas P, Field M, Andersen OJ, Gold MG, et al. 2017. Crystal structures of a $GABA_A$-receptor chimera reveal new endogenous neurosteroid-binding sites. *Nat. Struct. Mol. Biol.* 24:977–85
96. Chen Q, Wells MM, Arjunan P, Tillman TS, Cohen AE, et al. 2018. Structural basis of neurosteroid anesthetic action on $GABA_A$ receptors. *Nat. Commun.* 9:3972
97. Miller PS, Scott S, Masiulis S, De Colibus L, Pardon E, et al. 2017. Structural basis for $GABA_A$ receptor potentiation by neurosteroids. *Nat. Struct. Mol. Biol.* 24:986–92
98. Liu S, Xu L, Guan F, Liu YT, Cui Y, et al. 2018. Cryo-EM structure of the human $\alpha5\beta3$ $GABA_A$ receptor. *Cell Res.* 28:958–61
99. Phulera S, Zhu H, Yu J, Claxton DP, Yoder N, et al. 2018. Cryo-EM structure of the benzodiazepine-sensitive $\alpha1\beta1\gamma2S$ tri-heteromeric $GABA_A$ receptor in complex with GABA. *eLife* 7:e39383
100. Zhu S, Noviello CM, Teng J, Walsh RM Jr., Kim JJ, Hibbs RE. 2018. Structure of a human synaptic $GABA_A$ receptor. *Nature* 559:67–72
101. Walters RJ, Hadley SH, Morris KD, Amin J. 2000. Benzodiazepines act on $GABA_A$ receptors via two distinct and separable mechanisms. *Nat. Neurosci.* 3:1274–81
102. Kobilka BK, Deupi X. 2007. Conformational complexity of G-protein-coupled receptors. *Trends Pharmacol. Sci.* 28:397–406

103. Pierce KL, Premont RT, Lefkowitz RJ. 2002. Seven-transmembrane receptors. *Nat. Rev. Mol. Cell Biol.* 3:639–50
104. Oldham WM, Hamm HE. 2008. Heterotrimeric G protein activation by G-protein-coupled receptors. *Nat. Rev. Mol. Cell Biol.* 9:60–71
105. Santos R, Ursu O, Gaulton A, Bento AP, Donadi RS, et al. 2017. A comprehensive map of molecular drug targets. *Nat. Rev. Drug Discov.* 16:19–34
106. Carpenter B, Nehme R, Warne T, Leslie AG, Tate CG. 2016. Structure of the adenosine A_{2A} receptor bound to an engineered G protein. *Nature* 536:104–7
107. Rasmussen SG, DeVree BT, Zou Y, Kruse AC, Chung KY, et al. 2011. Crystal structure of the β2 adrenergic receptor–Gs protein complex. *Nature* 477:549–55
108. Tsai CJ, Pamula F, Nehme R, Muhle J, Weinert T, et al. 2018. Crystal structure of rhodopsin in complex with a mini-G_o sheds light on the principles of G protein selectivity. *Sci. Adv.* 4:eaat7052
109. Ghosh E, Kumari P, Jaiman D, Shukla AK. 2015. Methodological advances: the unsung heroes of the GPCR structural revolution. *Nat. Rev. Mol. Cell Biol.* 16:69–81
110. Chun E, Thompson AA, Liu W, Roth CB, Griffith MT, et al. 2012. Fusion partner toolchest for the stabilization and crystallization of G protein–coupled receptors. *Structure* 20:967–76
111. Cho KH, Husri M, Amin A, Gotfryd K, Lee HJ, et al. 2015. Maltose neopentyl glycol-3 (MNG-3) analogues for membrane protein study. *Analyst* 140:3157–63
112. Aherne M, Lyons JA, Caffrey M. 2012. A fast, simple and robust protocol for growing crystals in the lipidic cubic phase. *J. Appl. Crystallogr.* 45:1330–33
113. Warren AJ, Axford D, Paterson NG, Owen RL. 2016. Exploiting microbeams for membrane protein structure determination. *Adv. Exp. Med. Biol.* 922:105–17
114. Zhang X, Stevens RC, Xu F. 2015. The importance of ligands for G protein–coupled receptor stability. *Trends Biochem. Sci.* 40:79–87
115. Lebon G, Warne T, Tate CG. 2012. Agonist-bound structures of G protein–coupled receptors. *Curr. Opin. Struct. Biol.* 22:482–90
116. Scheerer P, Park JH, Hildebrand PW, Kim YJ, Krauss N, et al. 2008. Crystal structure of opsin in its G-protein-interacting conformation. *Nature* 455:497–502
117. Rasmussen SG, Choi HJ, Fung JJ, Pardon E, Casarosa P, et al. 2011. Structure of a nanobody-stabilized active state of the β_2 adrenoceptor. *Nature* 469:175–80
118. dal Maso E, Glukhova A, Zhu Y, Garcia-Nafria J, Tate CG, Atanasio S, et al. 2019. The molecular control of calcitonin receptor signaling. *ACS Pharmacol. Trans. Sci.* 2:31–51
119. Zhang Y, Sun B, Feng D, Hu H, Chu M, et al. 2017. Cryo-EM structure of the activated GLP-1 receptor in complex with a G protein. *Nature* 546:248–53
120. Kang Y, Kuybeda O, de Waal PW, Mukherjee S, Van Eps N, et al. 2018. Cryo-EM structure of human rhodopsin bound to an inhibitory G protein. *Nature* 558:553–58
121. Koehl A, Hu H, Maeda S, Zhang Y, Qu Q, et al. 2018. Structure of the μ-opioid receptor-G_i protein complex. *Nature* 558:547–52
122. Krishna Kumar K, Shalev-Benami M, Robertson MJ, Hu H, Banister SD, et al. 2019. Structure of a signaling cannabinoid receptor 1-G protein complex. *Cell* 176:448–58.e12
123. McLatchie LM, Fraser NJ, Main MJ, Wise A, Brown J, et al. 1998. RAMPs regulate the transport and ligand specificity of the calcitonin-receptor-like receptor. *Nature* 393:333–39
124. Koehl A, Hu H, Feng D, Sun B, Zhang Y, et al. 2019. Structural insights into the activation of metabotropic glutamate receptors. *Nature* 566:79–84
125. Dore AS, Okrasa K, Patel JC, Serrano-Vega M, Bennett K, et al. 2014. Structure of class C GPCR metabotropic glutamate receptor 5 transmembrane domain. *Nature* 511:557–62
126. Wu H, Wang C, Gregory KJ, Han GW, Cho HP, et al. 2014. Structure of a class C GPCR metabotropic glutamate receptor 1 bound to an allosteric modulator. *Science* 344:58–64
127. Kunishima N, Shimada Y, Tsuji Y, Sato T, Yamamoto M, et al. 2000. Structural basis of glutamate recognition by a dimeric metabotropic glutamate receptor. *Nature* 407:971–77
128. Shaik MM, Peng H, Lu J, Rits-Volloch S, Xu C, et al. 2019. Structural basis of coreceptor recognition by HIV-1 envelope spike. *Nature* 565:318–23

129. Kotev M, Pascual R, Almansa C, Guallar V, Soliva R. 2018. Pushing the limits of computational structure-based drug design with a cryo-EM structure: the Ca^{2+} channel $\alpha 2\delta$-1 subunit as a test case. *J. Chem. Inf. Model.* 58:1707–15
130. Muller H, Jin J, Danev R, Spence J, Padmore H, Glaeser RM. 2010. Design of an electron microscope phase plate using a focused continuous-wave laser. *New J. Phys.* 12:073011
131. Dandey VP, Wei H, Zhang Z, Tan YZ, Acharya P, et al. 2018. Spotiton: new features and applications. *J. Struct. Biol.* 202:161–69